THE JOURNAL OF BIOLOGICAL CHEMISTRY VOL. 286, NO. 46, pp. 40331–40342, November 18, 2011

The Leucine Zipper Putative Tumor Suppressor 2 Protein LZTS2 Regulates Kidney Development[S]

Received for publication, September 7, 2011 Published, JBC Papers in Press, September 26, 2011, DOI 10.1074/jbc.M111.302059

Yue Peng[‡§], Curtis Clark[‡], Richard Luong[¶], William H. Tu[‡], Jane Lee[‡§], Daniel T. Johnson[‡§], Amrita Das[‖], Thomas J. Carroll[‖], and Zijie Sun[‡§1]

From the Departments of [‡]Urology, [§]Genetics, and [¶]Comparative Medicine, Stanford University School of Medicine, Stanford, California 94305-5328 and the [‖]Departments of Internal Medicine (Nephrology) and Molecular Biology, University of Texas Southwestern Medical Center, Dallas, Texas 75390

Background: The LZTS2 is a novel β-catenin-interacting protein, and its role in development and tumorigenesis is unknown.
Results: *Lzts2* KO mice show severe kidney and urinary tract developmental defects, including renal/ureteral duplication, hydroureter, and hydronephrosis.
Conclusion: LZTS2 plays a critical role in kidney and urinary tract development.
Significance: A novel mechanism by which LZTS2 regulates β-catenin mediated nephrogenesis is implicated.

Members of the leucine zipper putative tumor suppressor (LZTS) family play crucial roles in transcription modulation and cell cycle control. We previously demonstrated that LZTS2 functions as a novel β-catenin-interacting protein and represses β-catenin-mediated transcription on T-cell factor/lymphoid enhancing factor. Here, we investigate the biological role of LZTS2 using newly established *Lzts2* KO mice. Homozygosity for loss-of-function of the *Lzts2*-targeted allele resulted in severe kidney and urinary tract developmental defects, including renal/ureteral duplication, hydroureter, and hydronephrosis, which were visible prenatally. Altered ureteric bud outgrowth was identified in *Lzts2* null embryos. Further analysis indicated that β-catenin subcellular localization was altered in fibroblasts isolated from *Lzts2* null embryos. In addition, Wnt growth factor-induced β-catenin-mediated transcriptional activity was increased in *Lzts2* null fibroblasts, suggesting a direct role for Lzts2 in the Wnt signaling pathway. These data demonstrate a critical role of LZTS2 in renal development and implicate LZTS2 as a critical regulator of β-catenin-mediated nephrogenesis.

The leucine zipper putative tumor suppressor (*LZTS*) gene family encodes a group of closely related proteins involved in transcription modulation and cell cycle control (1). *Lzts1*/*Fez1* is located on chromosomal region 8p22 in humans and ubiquitously expressed in normal tissues (2). *Lzts1*/*Fez1* deficiency was associated with an increased incidence of both spontaneous and carcinogen-induced tumors in mice (3). The *Lzts2*/*Lapser1* gene was originally identified on the basis of homology with the *Lzts1* gene (1). Overall, 38% of the amino acid residues were identical, and 15% were conservative changes between the LZTS1 and LZTS2 proteins. The human *LZTS2* gene is located on chromosome 10 at 10q24.3, near 10q23.3 where PTEN, a tumor suppressor, was identified (4). LZTS2 is expressed in most normal tissues, with the highest abundance found in testis, prostate, and ovary (1, 5). Overexpression of exogenous LZTS2 displayed a repressive effect on cell proliferation in multiple human tumor cell lines (1). The third member of the LZTS family, *LZTS3*, was identified on human chromosome 20p13 and is mainly expressed in brain and kidney tissues (6).

We previously demonstrated that LZTS2 is a β-catenin-interacting protein and represses β-catenin and T-cell factor/lymphoid-enhancing factor-mediated transcription (5). A unique Rev-like leucine-rich, CRM1/exportin-regulated nuclear export signal sequence was identified within the C-terminal region of LZTS2. Through this nuclear export signal site, LZTS2 modulates the nuclear export of β-catenin in a manner dependent on leptomycin-B, a CRM1/exportin-α inhibitor. Expression of exogenous LZTS2 reduces the level of nuclear β-catenin, inhibits the transcriptional activity of β-catenin, and represses cell growth. The effect of LZTS2 on β-catenin was observed during human adipose tissue differentiation and synaptic cross-talk in neural tissue (7, 8). In addition, LZTS2 has been shown to associate with p80 karatin and inhibit central spindle formation by abrogating microtubule transportation (9, 10).

To investigate the biological role of LZTS2 *in vivo*, we took a loss-of-function approach by disrupting the *Lzts2* alleles in mice. *Lzts2* null mice developed to term without obvious prenatal or postnatal lethality. However, developmental defects in the kidney and urinary tract including renal/ureteral duplication, hydroureter/hydronephrosis, and cystic dysplasia were observed in *Lzts2* null mice as early as embryonic day (E)[2] 17.5. Using *in situ* hybridization analysis, we demonstrated that *Lzts2* was expressed in Wolffian duct-, ureteric bud (UB)-, and

[S] The on-line version of this article (available at http://www.jbc.org) contains supplemental Fig. S1.

[1] To whom correspondence should be addressed: Depts. of Urology and Genetics, S287, Grant Bldg., Stanford University School of Medicine, Stanford, CA 94305-5328. Tel.: 650-498-7523; Fax: 650-725-8502; E-mail: zsun@stanford.edu.

[2] The abbreviations used are: E*n*, embryonic day *n*; UB, ureteric bud; MM, metanephric mesenchyme; ES, embryonic stem; CAKUT, congenital anomalies of the kidney and urinary tract; MEF, mouse embryonic fibroblast; OT, Topflash; OF, Foflash.

metanephric mesenchyme (MM)-derived tissues where β-catenin has also been shown to be expressed (11, 12). Abnormal Wolffian duct and ectopic UB formation was observed in *Lzts2* null embryos, predisposing to subsequent kidney and urinary tract malformation. These defects in *Lzts2* null mice appear similar to the abnormalities observed in β-catenin gain-of-function and loss-of-function mutations (13, 14). Further analysis indicated that the subcellular localization and transcriptional activity of β-catenin were altered in *Lzts2* null mice, suggesting that LZTS2 is a critical regulator of β-catenin during kidney and urinary tract development.

EXPERIMENTAL PROCEDURES

Gene Targeting and Genotyping—The mouse *Lzts2* gene is located on chromosome 19 and is organized into five exons spanning an ~11.8-kb region. Mouse BAC clones (RPCI22 129S6/SvEvTac) containing the mouse *Lzts2* gene were identified by PCR approaches. A PGK-neomycin cassette flanked by *loxP* and *FRT* sites was inserted upstream of exon 2 containing the translation initiating codon. A third loxP site was inserted downstream of exon 3 using Red/ET recombineering. The linearized construct was electroporated into iTL BA1 hybrid (C57BL/6 × 129/SvEv) embryonic stem cells (inGenious Targeting Laboratory, New York). Correctly recombined ES clones were identified by PCR using primer sets for the Neo cassette (Neo1, 5′-agcgcatcgccttctatcgccttc-3′), flanking sequences (A2, 5′-tctgagtttgaggcccacctatgg-3′), and the loxP site (5′agggtgttagtttagcaag-3′). Two independent ES clones that were heterozygous for the targeted alleles were identified. They were injected into C57BL/6 blastocysts and implanted into pseudopregnant recipients. Germ line transmission was achieved by backcrossing male chimeras to wild type C57BL/6J female mice. To generate the whole body knock-outs of *Lzts2* mice, $Lzts2^{floxneo}$ mice were first bred with *β-Actin/Flp* mice to remove the PGK-neomycin cassette (15) and then bred with *EIIa-Cre* mice (16). Mice with *Lzts2* heterozygous allele ($Lzts2^{+/-}$) were backcrossed with C57BL/6J mice for at least five generations before being intercrossed to generate mice homozygous for the null allele ($Lzts2^{-/-}$). This study was carried out in strict accordance with the recommendations in the Guide for the Care and Use of Laboratory Animals of the National Institutes of Health. All of the animal experiments performed in this study were approved by the ethics committee of the Administrative Panel on Laboratory Animal Care at Stanford University.

Mouse tail tips or embryo yolk sacs were incubated in lysis buffer (Viagen Biotech, Los Angeles, CA) supplemented with 400 μg/ml of proteinase K (Roche Applied Science) overnight at 55 °C and then were heat-inactivated at 85 °C for 45 min. Lysates were analyzed with three primers to identify wild type and mutant alleles: common forward primer, 5′-TACCATCTGAGTTGCTGATTGC-3′; wild type reverse primer, 5′-AGAGAGGAAGGAATGGGAGATC-3′; and deleted reverse primer, 5′-CACAAGGAATGCTCCAACCCTG-3′. PCR was carried out at 94 °C for 5 min and then for 35 cycles of 94 °C for 45 s, 60 °C for 45 s, and 72 °C for 80 s, followed by a final step at 72 °C for 10 min.

Southern, Northern, and Western Blot Analyses—Genomic DNA samples were isolated from yolk sacs of E13.5 mouse embryos. Ten μg of DNA from each sample was digested by HindIII, electrophoresed on 0.8% agarose gel, blotted onto nylon membrane, and then hybridized with the ^{32}P-labeled probe derived from exon 4. Total RNA samples were isolated from E13.5 whole mouse embryos and used for poly(A) RNA purification. Northern blot analysis was carried out as described previously (17). Briefly, 1.5 μg of poly(A) RNA samples were electrophoresed on 1% formalin-denatured agarose gel, blotted onto nylon membrane, and then hybridized with a DNA fragment spanning the junction region between exon 4 and exon 5. For Western blot analysis, different aged mouse embryos were cut into small pieces, homogenized, and then extracted in buffer containing 50 mM Tris-HCl, pH 8.0, 1% Nonidet P-40, 150 mM NaCl, 0.5% sodium deoxycholate, 0.1% SDS, 10 μg/ml aprotinin, 10 μg/ml leupeptin, 10 mM phenylmethylsulfonyl fluoride, and 0.5 mM sodium orthovanadate. Whole cell lysates were cleared by centrifugation, and supernatants were subjected to SDS-PAGE analysis. Proteins were transferred to nitrocellulose membranes, blocked with 5% milk, and immunoblotted using appropriate primary and species-specific horseradish peroxidase-conjugated secondary antibodies. A polyclonal LZTS2 antibody (5) was used at a 1:50 dilution. The antibody against β-tubulin (clone DM1A; Neomarkers, Freemont, CA), β-catenin, or Ku86 (Santa Cruz Biotechnology) was used at 1:1,000 and 1:300 or 1:500 dilutions, respectively.

Whole Mount and Section in Situ Hybridization, Immunohistochemistry, and Histology—Embryos and kidneys at various stages were isolated and fixed overnight in 4% paraformaldehyde in PBS at 4 °C. The experimental procedure for *in situ* hybridization was performed as reported previously (18). Two DNA fragments for the mouse Lzts2 N-terminal region (between amino acids 54 and 192) or the C-terminal region (between amino acids 355 and 533) were generated by PCR with specific primers and were cloned into pGEM T Easy vector (Promega). Either sense or antisense RNA probes were generated using the Roche DIG RNA labeling kit (Roche Applied Science). RNA probes for c-*Ret*, *Pax2*, *Wnt11*, *Gdnf*, (19), and *Gata3* (20) were also generated and used in the analyses. Images were acquired on a Leica dissecting microscope (model $MZ9_5$) using a Zeiss Axiocam and Axiovision software.

Mouse tissues were fixed in 10% neutral-buffered formalin and processed into paraffin for immunohistochemistry. Samples were cut into 5-μm sections, deparaffinized in xylene, and rehydrated using a decreasing ethanol gradient followed by PBS. Tissues were then blocked with 3% hydrogen peroxide in methanol to inhibit endogenous peroxidase activity and nonspecific antibody binding, respectively. Samples were exposed to a 1:100 dilution of rabbit polyclonal anti-LZTS2 antibody, 1:1000 dilution of anti-β-catenin antibody (Santa Cruz Biotechnology), 1:3000 dilution of anti-Ki67 antibody, or 1:500 dilution of anti-E-cadherin antibody in 1% goat serum overnight at 4 °C. The slides were then incubated with biotinylated antirabbit/antimouse antibody solution (Biogenex, San Ramon, CA) and streptavidin peroxidase (Lab Vision, Fremont, CA) for 30 min each and then visualized with 3,3′-diaminobenzidine

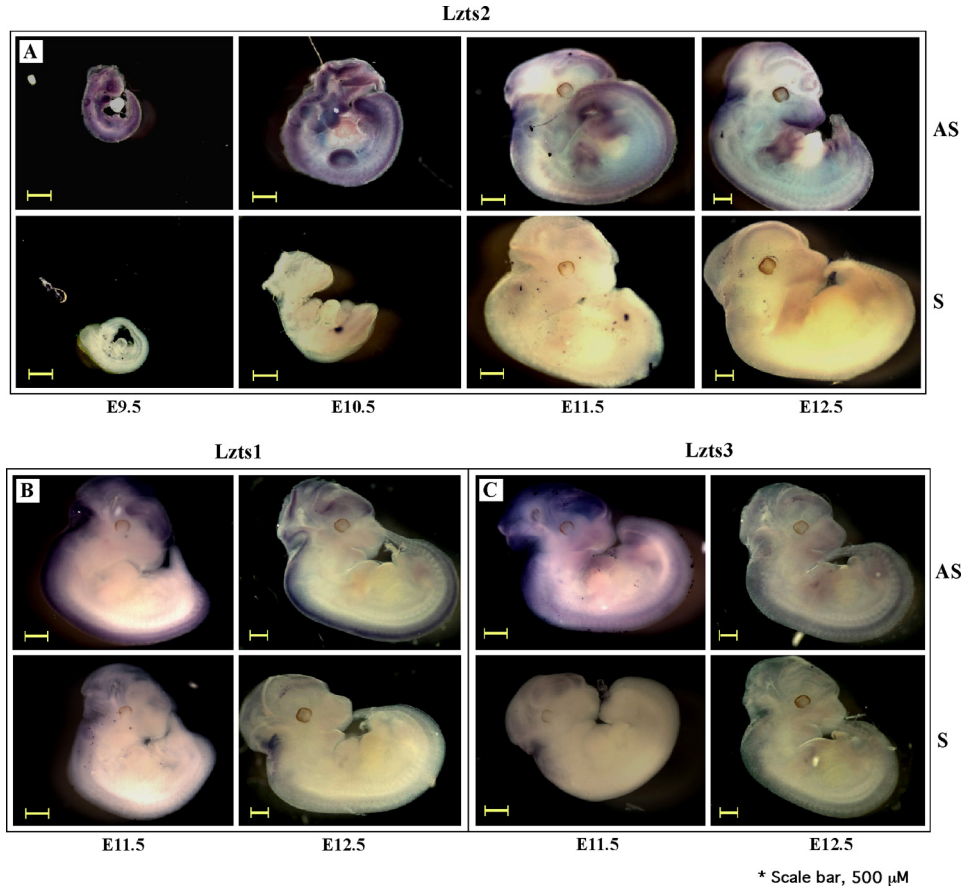

FIGURE 1. **Expression of *Lzts2* during mouse development.** *A*, wild type embryos were isolated at E9.5, E10.5, E11.5, and E12.5 and subjected to *in situ* hybridization using a RNA probe specific for the mouse Lzts2 sequence (amino acids 355–533) as described under "Experimental Procedures." The magnification settings were adjusted according to the stage so that the embryo filled the field of view. *Top panel*, antisense probe (*AS*); *bottom panel*, sense probe (*S*). *Scale bars*, 500 μm. *B* and *C*, wild type embryos were isolated at E11.5, and E12.5 and subjected to *in situ* hybridization using a RNA probe specific either for the *Lzts1* sequence between amino acids 301 and 436 (*B*) or the *Lzts3* sequence between amino acids 284 and 444 (*C*). *Top panel*, antisense probe (*AS*); *bottom panel*, sense probe (*S*). *Scale bars*, 500 μm.

substrate solution (DAKO Corp., Carpinteria, CA) in PBS containing 0.3% hydrogen peroxide. The slides were subsequently counterstained with 5% (w/v) Harris hematoxylin. For histological analysis, 5-μm-thick serial sections were processed from xylene to water through a decreasing ethanol gradient, stained with hematoxylin and eosin, and processed back to xylene through an increasing ethanol gradient. Coverslips were mounted using Permount mounting medium (Fisher).

Luciferase Reporter Assays—Mouse embryonic fibroblasts were isolated and maintained as described previously (21). Wnt3A conditioned medium or L medium was prepared according to the previous report (22), and transient transfection and luciferase assays were performed using Topflash (pGL3-OT) and Foflash (pGL3-OF) luciferease reporters as described previously (5).

RESULTS

Expression of Lzts2 during Development—Using *in situ* hybridization approaches, we first assessed expression of *Lzts2* during mouse development using wild type embryos. As shown in Fig. 1*A* (*top row*), *Lzts2* expression was detected throughout the embryo at E9.5 by an antisense probe derived from the C terminus of the *Lzts2* cDNA. The areas of intense staining include the forebrain, midbrain, hindbrain, and mandibular brachial arches. In addition, *Lzts2* displayed widespread dorsal expression, including the tail bud, which persisted throughout development and appeared to become more localized to the periphery of the embryo at later stages. Craniofacial expression of *Lzts2* was apparent at all stages examined and became more localized to the periphery of the embryo as development progressed. Interestingly, the embryo forelimbs and hindlimbs also displayed significant staining with the *Lzts2* antisense probe. Similar staining patterns were observed in E9.5 to E12.5 embryos with an N-terminal *Lzts2* antisense probe (data not shown). However, there was no staining with corresponding sense probes used as negative controls (Fig. 1*A*, *bottom row*).

To fully evaluate the effect of LZTS proteins in development, we also assessed the expression of *Lzts1* and *Lzts3* in different stages of mouse embryos. As shown in Fig. 1*B*, *Lzts1* expression was detected on E11.5 and E12.5 embryos with an antisense probe derived from the C terminus of *Lzts1*. In contrast to ubiquitous expression of *Lzts2*, the staining of *Lzts1* was limited to the forebrain, midbrain, hindbrain, and dorsal area. *Lzts3* expression was detected on E11.5 and E12.5 embryos at much lower levels with an antisense probe derived from the C terminus of *Lzts3*. Weak staining was also observed in the brain, dorsal area, craniofacial area, and limbs. We observed similar

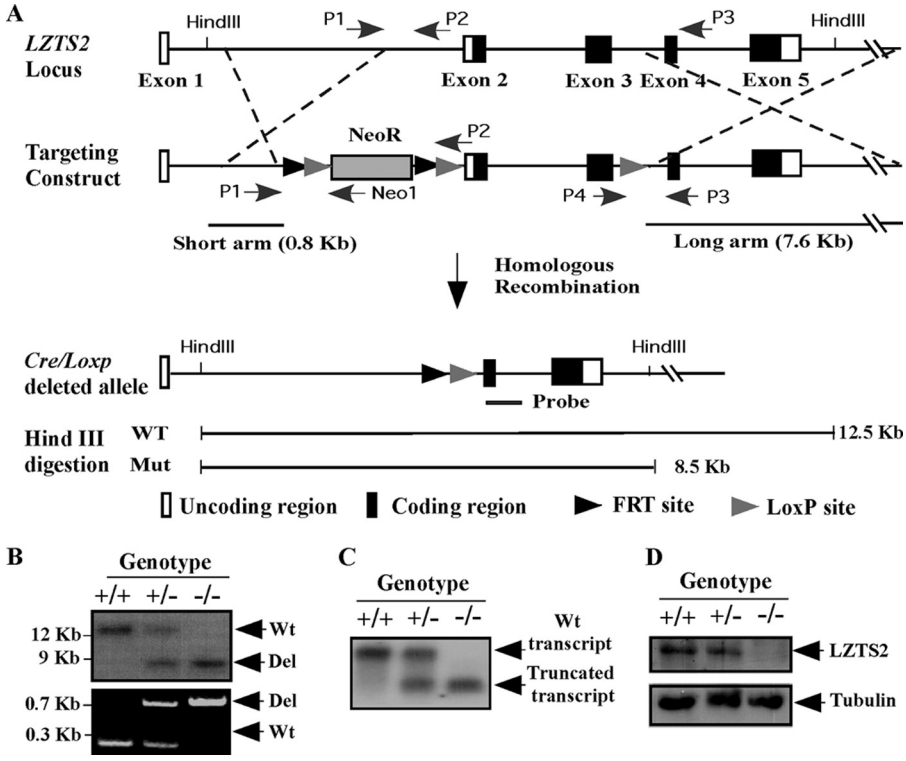

FIGURE 2. **Disruption of the *Lzts2* gene in mouse ES cells.** *A*, the targeting construct used to disrupt the endogenous *Lzts2* gene in ES cells is shown in the figure. Briefly, a PGK-neomycin cassette flanked by *loxP* and *FRT* sites was inserted upstream of exon 2 containing the translation start codon. A third *loxP* site was inserted downstream of exon 3 using Red/ET recombineering. The hypothetical crossovers between the endogenous *Lzts2* allele and the targeting construct are indicated by the *dashed lines*. Correctly recombined ES clones were identified by PCR using primer sets for the Neo cassette (Neo1), flanking sequences (P1), and the downstream loxP site (P3/P4). The desired disruption of *Lzts2* allele can be induced by the *Cre/loxP* system. *B*, mouse genomic DNA samples were isolated from E11.5 mouse embryos. Ten μg of genomic DNA were digested by HindIII, electrophoresed on 0.8% agarose gel, blotted onto nylon membrane, and hybridized to a ^{32}P-labeled probe located on exon 4 (*top panel*). The above genomic DNA samples were also used for genotyping PCR (*bottom panel*). Two pairs of primers were used to distinguish the WT (P4/P3) or deleted (KO) allele (P1/P3). *C*, total RNA samples were isolated from E11.5 embryos and purified by oligo(dT)-conjugated cellulose for poly(A) RNA. Approximately 2 μg of poly(A) RNA were electrophoresed on 1% formalin-denatured agarose gel, blotted onto nylon membrane, and hybridized to the ^{32}P-labeled probe covering the junction region of exon 4 and exon 5. *D*, total cell lysates were prepared from E11.5 mouse embryos and analyzed by Western blot with a LZTS2 antibody.

staining patterns when the *Lzts1* or *Lzts3* N-terminal probes were used (data not shown). No staining was observed with sense probes (Fig. 1, *B* and *C*, *bottom rows*).

Disruption of the Lzts2 Gene in Mouse ES Cells and Embryos—To investigate the biological role of LZTS2 *in vivo*, we took a loss-of-function approach by generating an *Lzts2*-deficient mouse strain. The mouse *Lzts2* gene is localized to chromosome 19 and organized into five exons spanning an ~11.8-kb region of genomic DNA (Fig. 2*A*). The *Lzts2* whole body knock-out mice were generated through breeding *Lzts2* floxed mice with *β-Actin/Flp* (15) and *EIIa-Cre* mice (16), as detailed under "Experimental Procedures" (Fig. 2*A*). Further intercrossing between *Lzts2* heterozygous mice ($Lzts2^{+/-}$) produced homozygous knock-out mice ($Lzts2^{-/-}$). Mouse genomic DNA samples were isolated from E13.5 embryos and analyzed by Southern blot with a probe derived from exon 4 as indicated in Fig. 2*A*. An 8.5- or 12.5-kb fragment for the deleted or wild type allele was detected in different genotypes of embryos accordingly (Fig. 2*B*, *top panel*). Using specific primers (P1, P3, and P4; Fig. 2*A*), we also assessed the genotypes of embryos using genomic PCR analysis (Fig. 2*B*, *bottom panel*). Total RNA samples were isolated from E11.5 embryos and analyzed by Northern blot using a probe spanning the junction region between exons 4 and 5 (Fig. 2*C*). Finally, we evaluated expression of Lzts2 proteins using an anti-Lzts2 antibody in Western blot analyses. As shown in Fig. 2*D*, Lzts2 expression was detected in wild type and, to a lesser extent, in heterozygous embryos but was absent in *Lzts2* null embryos. Taken together, the above data demonstrate that Lzts2 protein expression was disrupted in *Lzts2* null mice.

$Lzts2^{-/-}$ Mice Exhibit Kidney and Urinary Tract Anomalies—Homozygous *Lzts2* KO mice were born at the expected Mendelian ratios. We did not observe significant postnatal lethality associated with *Lzts2* null mice. However, phenotypic analyses of $Lzts2^{-/-}$ mice between the ages of 4 and 12 months revealed abnormal urinary tract development in 20 of 28 (71%) mice (Table). Some of the typical gross kidney and urinary tract abnormalities that were frequently observed in *Lzts2* null mice are presented in Fig. 3*A*. They included left kidney hydronephrosis, mildly dilated and shortened left ureter with malformed left seminal vesicle (Fig. 3*A2*), right hydronephrosis and left uterus horn pyometra (Fig. 3*A3*), duplicated left kidney with mildly dilated and shortened ureters with left seminal vesicle ectasia (Fig. 3*A4*), mild left kidney hydronephrosis and dilated shortened left ureter with left seminal vesicle ectasia (Fig. 3*A5*), and bilateral hydronephrosis with duplicated right ureters (Fig. 3*A6*). Six of *Lzts2* null mice showed multiple kidneys and urinary tract abnormalities (Table 1). However, among 58 of

TABLE 1
Kidney and urinary tract abnormalities in *Lzts2* knockout mice

Genotype (Lzts2)	Total *n* of mice (*n* with abnormality)	Duplication of kidney and/or ureter	Hydronephrosis and/or hydroureter	Kidney cysts
+/+	Male 16 (0)	0	0	0
	Female 14 (0)	0	0	0
+/−	Male 30 (1) 3%	0	1	0
	Female 28 (0)	0	0	0
−/−	Male 16 (12) 75%[a]	5	7	2
	Female 12 (8) 67%[b]	4	5	2

[a] Two mice had more than two urinary abnormalities.
[b] Four mice had more than two urinary abnormalities.

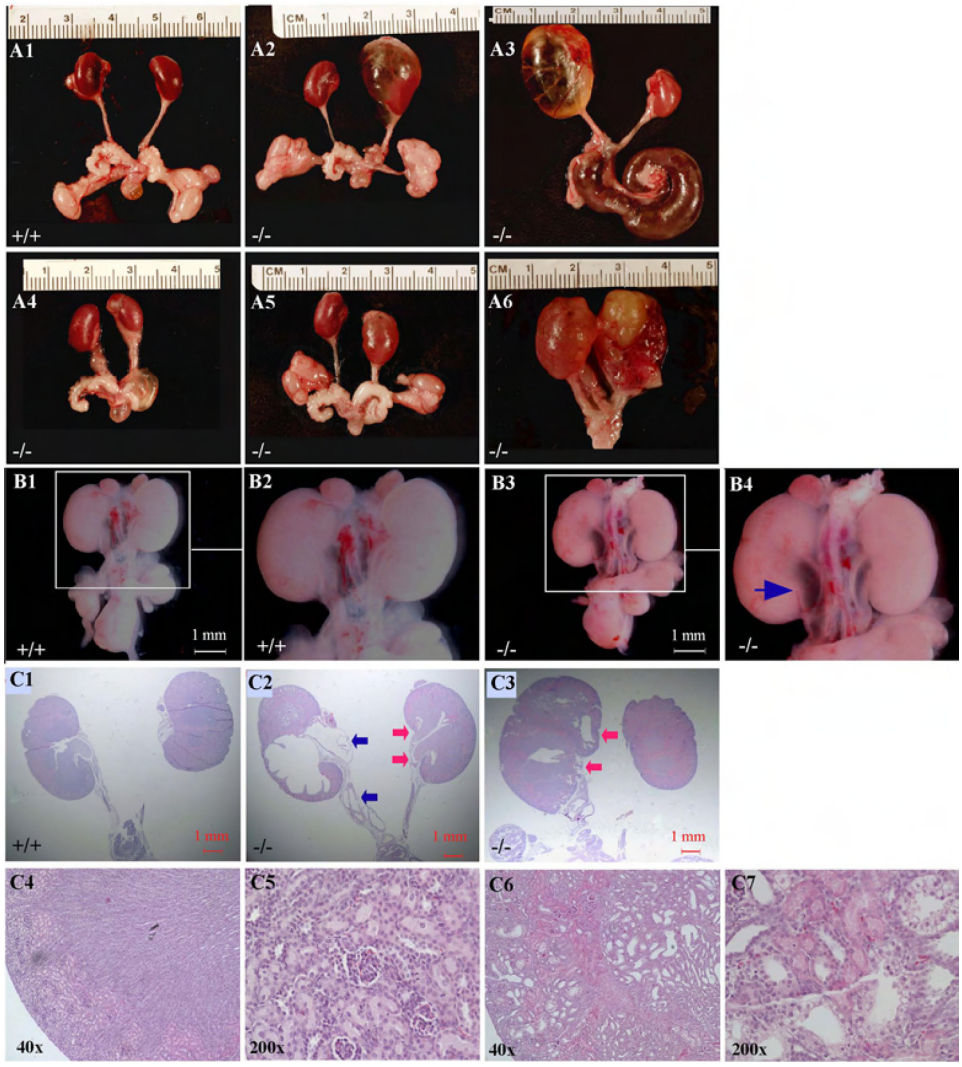

FIGURE 3. ***Lzts2* null mice exhibit kidney and urinary tract anomalies.** *A*, adult mice at 6–12 months old were examined for abnormalities, and representative images are shown. *A1*, normal urogenital tract including kidneys, ureters, seminal vesicles, and testicles was shown in a *Lzts2*$^{+/+}$ male mouse. *A2*, a *Lzts2* null male mouse had a normal right kidney, ureter, and seminal vesicle but had left kidney hydronephrosis, mildly dilated and shortened left ureter, and malformed left seminal vesicle. *A3*, a *Lzts2* null female mouse showed normal left kidney and ureter but right hydronephrosis and left uterine horn pyometra. *A4*, a *Lzts2* null *male* mouse showed duplicated left kidney with mildly dilated and shortened ureters and left seminal vesicle ectasia. *A5*, a *Lzts2* null male mouse showed normal right kidney and ureter, mild left kidney hydronephrosis, and dilated shortened left ureter with left seminal vesicle ectasia. *A6*, a *Lzts2* null female mouse showed bilateral hydronephrosis with duplicated right ureters. *B*, embryos at E17.5 were examined for gross urinary tract abnormalities and representative images were shown. *B1* and *B2*, urinary tract from a wild type embryo. *B3* and *B4*, urinary tract from a *Lzts2* null embryo revealed double ureters, accompanied by hydroureter and hydronephrosis (*blue arrow*). *C*, newborn mice were examined by histology for urinary tract abnormalities and representative sections were shown. *C1*, normal urinary tract from a *Lzts2*$^{+/+}$ neonate at lower magnification. *C2*, urinary tract from a *Lzts2* null neonate at lower magnification showed right kidney hydronephrosis and hydroureters (*blue arrows*) and left kidney duplex renal pelvises connected to double ureters (*red arrows*). *C3*, a *Lzts2* null neonate showed double renal pelvises in the right kidney (*red arrows*), in which the nephrogenic zones were not restricted to the cortex, indicating a duplex kidney. *C4* and *C5*, normal kidney tissues from the *Lzts2*$^{+/+}$ neonate (*C1*) were examined at 40× and 200× magnification. *C6* and *C7*, histological examination of the *Lzts2* null mouse kidney tissues (*C3*) with both 40× and 200× magnification was shown.

Lzts2$^{+/-}$ littermates, only one male mouse displayed mild unilateral hydronephrosis and hydroureter at an age of 20 weeks. No abnormality was observed in 30 wild type littermates (*Lzts2*$^{+/+}$). The above data provide the first line of evidence demonstrating an important role for *Lzts2* in kidney development.

Next, we examined the abnormalities in kidney and urinary tract in E17.5 *Lzts2* null embryos (Fig. 3, *B1* and *B3*, respectively). We observed double ureters, accompanied by hydroureter and hydronephrosis (Fig. 3, *B3* and *B4*), which suggests that the urinary tract abnormalities encountered in adult *Lzts2* null mice likely originated during embryonic development. Then we examined the histology of kidneys and ureters in wild type and *Lzts2* null neonates (Fig. 3, *C1*, *C2*, and *C3*, respectively). Microscopic analysis revealed a range of kidney and urinary abnormalities, including the left kidney with double renal pelvises (Fig. 3*C2*, *red arrows*) and the right kidney with hydroureter, which was accompanied by hydronephrosis and duplicated ureters (Fig. 3*C2*, *blue arrows*). In another *Lzts2* null neonate, we observed that duplicated ureters were connected to unilateral duplex kidneys (Fig. 3*C3*, *red arrows*). Specifically, the nephrogenic zones in the kidney of this null neonate were not restricted to the cortex but extended throughout the entire kidney, and there were two kidney primordia fused together. Microscopic examination of the *Lzts2* null kidney at higher magnifications (Fig. 3, *C6* and *C7*) showed abnormal histologic organization, including tubular dilation and a lack of glomerular structures, in comparison with the architecture in the normal kidney of an age- and sex-matched wild type control (Fig. 3, *C4* and *C5*). In addition, we observed that 4 of 21 (19.0%) *Lzts2* null newborns exhibited multiple macroscopic and microscopic kidney cysts (see Fig. 6). Taken together, the above data further elucidate an important role of Lzts2 in kidney and urinary tract development.

Expression of Lzts2 in Early Kidney Development—The data described above indicate that the defective phenotypes of *Lzts2* null mice in the kidney and urinary tract may be caused by budding of the ureter at aberrant positions along the nephric duct, also known as the Wolffian duct, or the mesonephric duct. To determine the role of *Lzts2* in regulating UB formation, we examined expression of *Lzts2* in E10.5 mouse kidney tissues using *in situ* hybridization approaches. c-Ret, a tyrosine kinase receptor, is weakly expressed in the Wolffian duct but is up-regulated in the ureteric bud tip (23). Using a c-Ret RNA probe, we located the Wolffian duct and UB in E10.5 wild type embryos by *in situ* hybridization (Fig. 4, *A* and *A′*). Intriguingly, *Lzts2* expression was also detected in the Wolffian duct of a wild type E10.5 embryo (Fig. 4, *B* and *B′*, *pink arrows*). By contrast, *Lzts2* expression was virtually undetectable in *Lzts2* null embryos (Fig. 4, *C* and *C′*). Gata3 expression has been shown at ureteric tips and trunks between E14.5 and E15.5 embryonic kidneys, which allows Gata3 to be used as a marker in the above structures (Fig. 4, *D*, *G*, and *J*). At E14.5, expression of *Lzts2* in wild type embryos appears ubiquitous in both UB and mesenchyme-derived tissues around the kidney. In addition, expression of Lzts2 was also observed in other tissues, including adrenal glands, bladder, testicles, etc. (Fig. 4*E*). Lzts2 staining was not detected in *Lzts2* null embryos as shown in the representative image (Fig. 4*F*). The Lzts2 staining in E15.5 embryos appeared to be more concentrated in ureteric buds, collecting ducts, cap mesenchyme, and renal vesicles (Fig. 4, *H* and *K*). There is no staining of Lzts2 with the same probe in *Lzts2* null kidney sections (Fig. 4, *I* and *L*). At E18.5, *Lzts2* expression pattern remained while kidney development proceeded in $Lzts2^{+/+}$ embryos (Fig. 4*M*). The above staining was decreased or completely absent in $Lzts2^{+/-}$ (Fig. 4*N*) or $Lzts2^{-/-}$ (Fig. 4*O*) littermates, respectively, which further confirms the specificity of the Lzts2 probe used in the experiments. To assess whether expression of other *Lzts* members changes to compensate for the loss of *Lzts2* in the *Lzts2* null mice, we evaluated expression of *Lzts1* and *Lzts3* in both E18.5 $Lzts2^{+/+}$ and $Lzts2^{-/-}$ embryos (Fig. 4, *P–S*). Although *Lzts1* was barely detected in kidneys, *Lzts3* was observed mainly at ureteric tips and ureteric trunks as well as with low expression in mesenchyme. The expression of *Lzts1* and *Lzts3* was not changed significantly between wild type and *Lzts2* null embryos. Taken together, the above data demonstrate expression of *Lzts2* in different stages of mouse kidneys, supporting its important role in kidney development.

Lzts2 Null Animals Exhibited Abnormal Wolffian Duct and Ectopic Ureteric Bud Formation—The range of abnormal kidney and urinary tract phenotypes in *Lzts2* null mice shares similar pathological characteristics to those noted in human congenital anomalies of the kidney and urinary tract (CAKUT). Ectopic budding of the ureter from the Wolffian duct is usually the first ontogenic misstep that leads to CAKUT (24). Mouse metanephric kidney development begins at approximately E10.5 to E11, after the Wolffian duct, which derives from the intermediate mesoderm, extends caudally along the body axis, and produces an outgrowth called the UB (25). In this study, we visualized expression of *c-Ret* and *Lzts2* in the Wolffian duct and UB in E10.5 wild type embryos, suggesting a potential role of *Lzts2* in early kidney development (Fig. 4, *A* and *B*). Using whole mount *in situ* approaches, we evaluated Wolffian duct and UB morphology in E10.5 to E11.5 *Lzts2* null embryos with a specific probe for c-*Ret* (26, 27). At E10.5, the entire posterior end of the Wolffian duct was much broader (*yellow arrowhead*) and bifurcated (*red arrow*) in *Lzts2* null embryos compared with a wild type littermate (Fig. 5, *A2 versus A1*, *red arrows*). By E11.5, the single wild type ureteric bud had extended into the MM and acquired a distinctive shape (Fig. 5*A3*, *red arrow*). By contrast, *Lzts2* null embryos showed ectopic UBs (Fig. 5*A4*, *yellow arrowhead*), which were more anterior to the normal bud location (the red arrow) but still confined to the area of the normal metanephric mesenchyme. To test whether the expanded c-Ret expression equated to expanded function, we examined the expression of the downstream target, Wnt11. In contrast to c-Ret, Wnt11 expression is normally restricted to the ureteric bud sites at E10.5 (Fig. 5*B1*). However, we saw clear evidence of ectopic ureteric buds in Lzts2 null embryos at E10.5 and E11.5 (Fig. 5, *B2* and *B4*, *arrows*).

Glial cell line-derived neurotrophic factor (Gdnf) is expressed in the nephrogenic mesenchyme and plays an essential role in induction of UB through its receptor, c-Ret (28). Given the abnormal patterning of the UB in *Lzts2* null mice, we examined expression of *Gdnf* at E10.5 and E11.5 during UB formation. We observed that *Gdnf* stained the metanephric mesenchyme in *Lzts2* null embryos (Fig. 5, *C1–C4*). There is no significant difference in the expression domain of GDNF in wild type or *Lzts2* null embryos at E10.5 or E11.5 after normalizing according to somite number. At E11.5, when the single normal UB is expected to invade the mesenchyme, a split mes-

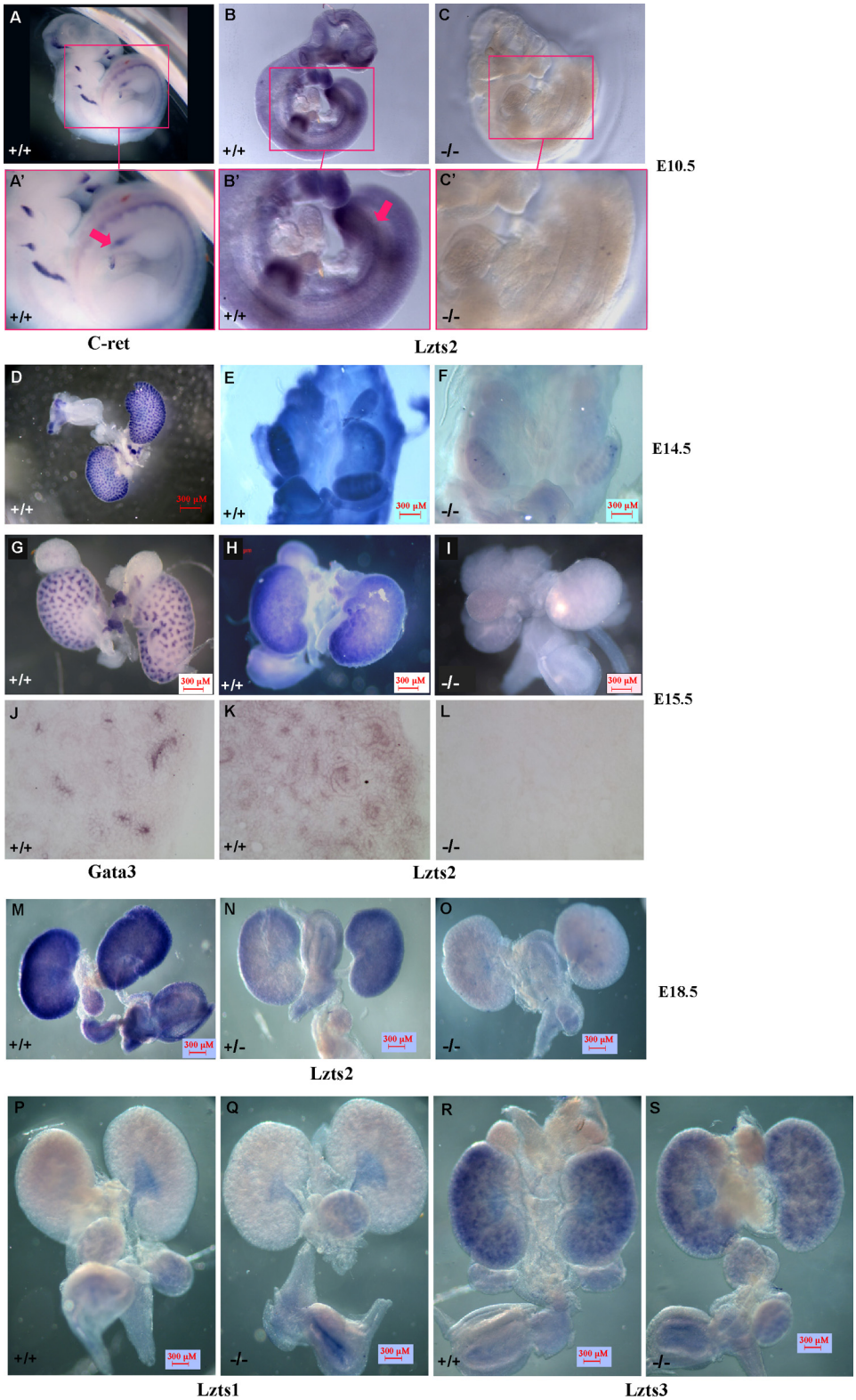

FIGURE 4. ***Lzts2* expresses in ureteric bud and metanephric mesenchyme-derived tissues during kidney development.** *A* and *A'*, a probe for c-Ret was used in the *in situ* hybridization to locate the Wolffian duct and UB in E10.5 wild type embryos. *B* and *B'*, *Lzts2* expression was detected with a specific RNA probe for Lzts2 using *in situ* hybridization the Wolffian duct of a wild type E10.5 embryo. The *arrow* indicates the Wolffian duct. *C* and *C'*, a *Lzts2* null littermate was assessed using *in situ* hybridization approach as described for *B*. *D*, *G*, and *J*, a specific probe for Gata3 was generated and used to detect Gata3 expression in ureteric tips and ureteric trunks of E14.5 and E15.5 embryonic kidneys by whole mount and section *in situ* hybridization. *E* and *F*, the expression of *Lzts2* was assessed in both UB and mesenchyme-derived tissues in the kidney of a wild type (*E*) or *Lzts2* null (*F*) E15.5 embryo using *in situ* hybridization. *H* and *K*, *Lzts2* expression was examined in kidney and urinary tissues of a wild type E15.5 embryo using whole mount (*H*) or section (*K*) *in situ* hybridization. *I* and *L*, an E15.5 *Lzts2* null embryo was examined as described above. *M–O*, *Lzts2* expression was examined in E18.5 wild type, *Lzts2*$^{+/-}$, and *Lzts2*$^{-/-}$ embryos using the same RNA probe as described above. *P* and *Q*, *Lzts1* expression was assessed in E18.5 urogenital tissues from *Lzts2*$^{+/+}$ and *Lzts2* null embryos. *R* and *S*, Lzts3 expression was examined in E18.5 urogenital tissues from *Lzts2*$^{+/+}$ and *Lzts2* null embryos.

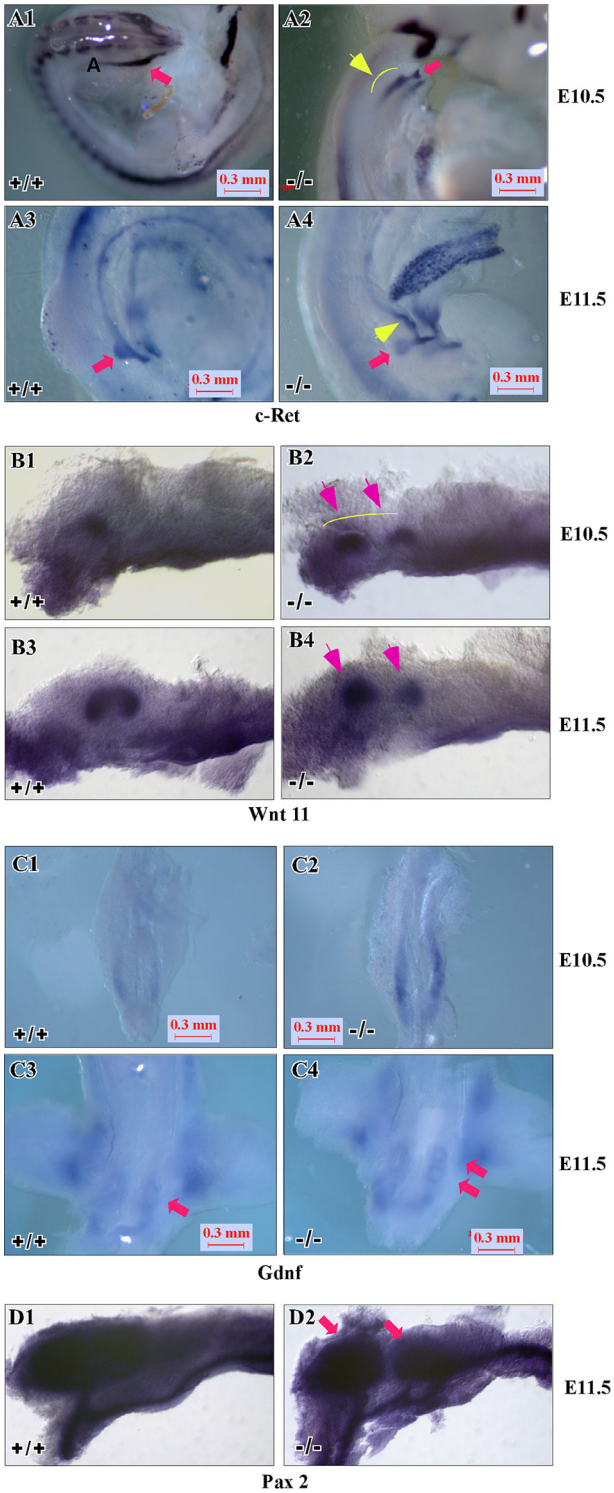

FIGURE 5. ***Lzts2* null animals exhibited abnormal Wolffian duct and ectopic ureteric bud formation.** *A*, staining for *c-Ret* in wild type and *Lzts2* null E10.5 and 11.5 embryos. The *arrow* indicates a normal budding UB in E10.5 embryos (*A1*). Staining for c-Ret in a *Lzts2* null embryo at E10.5 shows a much broader outgrowing UB (*yellow arrowhead*) and a bifurcated posterior end of the Wolffian duct (*red arrow*, *A2*). Staining for c-Ret shows that the single normal UB had extended into the MM and acquired a distinctive shape in a wild type E11.0 embryo (*red arrow*, *A3*). Staining for c-Ret in a *Lzts2* null embryo at E11.5 shows both ectopic UBs (*yellow arrowhead*) more anterior to the normal bud (*red arrow*). *B*, staining for Wnt11 in wild type and *Lzts2* null E10.5 and 11.5 embryos. The ectopic ureteric buds are marked with *arrows*. *C*, staining for Gdnf in wild type and *Lzts2* null E10.5 and 11.5 embryos. At E11.5, the wild type embryo shows the mesenchyme (*single arrow*) invaded by enchyme stained by the Gdnf probe was observed in the *Lzts2* null mutant (Fig. 5*C4*, *double arrows*), but this phenotype appears to be a consequence of the ectopic ureteric buds and not the effect. To confirm our observations, we examined expression of *Pax2*, a gene that is expressed in both the urteric bud and mesenchyme, in wild type and *Lzts2* null embryos. As shown in Fig. 5*D*, ectopic ureteric buds clearly appear in *Lzts2* null embryos (*arrows*). These data suggest that the ectopic ureteric buds that form in Lzts2 mutants are the result of a misinterpretation of the GDNF/Ret signal within the Wolffian duct.

Lzts2 Null Mice Displayed Cystic Renal Dysplasia—In this study, we also identified microscopic and macroscopic renal cysts in kidney tissues of 4 of 21 *Lzts2* null mice. As shown in Fig. 6*A*, a representative focal macroscopic renal polycystic lesion was observed in the upper pole of the kidney of a newborn *Lzts2* null mouse (Fig. 6, *A1* and *A2*, *yellow arrows*). Histological analysis showed multiple renal cyst formation in parenchyma (Fig. 6, *B1* and *B2*). Using dolichos biflorus agglutinin (FITC-labeled) staining, we demonstrated that these multiple renal cysts were mainly derived from the collecting ducts in the kidney of *Lzts2* null mice (Fig. 6, *C1* and *C2*). We did not observe similar pathological changes in wild type mice (Fig. 6, *B3* and *C3*). Because the collecting system develops from the UB, the above observation suggests that defects in the embryonic ureteric epithelium may result in cyst formation. As shown in Fig. 6*A2*, the renal cysts were present in the upper pole of the *Lzts2* null kidney and attached to the hydroureter (indicated by yellow arrow), suggesting that ureteric obstruction likely contributed to the renal cyst formation. Alterations in adhesive properties of tubular epithelial cells have been suggested to associate with renal cystic lesions (29). Therefore, we assessed the expression of E-cadherin, a key cellular component of adhering junctions, in *Lzts2* null cystic epithelia. Positive staining in ureteric epithelium was observed in the wild type mouse kidney tissue (Fig. 6*D1*). We observed that large patches of cells lining the cysts showed loss of or reduced expression of E-cadherin in *Lzts2* null kidney tissues, suggesting that they had undergone alterations from their normal adhesive properties (Fig. 6, *D2* and *D3*, *two red asterisks*). These E-cadherin negative cells appeared to be disorganized and loosely attached to each other, which was in contrast to the relative normal branching ureteric epithelium consisting of a single layer of epithelial cells in the same tissues (Fig. 6, *D2* and *D3*, *one red asterisk*). We also examined the expression of Ki67, a proliferation marker, in the above kidney tissues. Typical nuclear staining of Ki67 was shown in epithelial cells lining renal cysts in *Lzts2* null neonate kidneys (Fig. 6, *E2* and *E3*). In contrast, Ki67-positive cells were mainly present in undifferentiated mesenchyme, condensing mesenchyme, and renal vesicles within the nephrogenic zone immediately under the renal capsule in normal neonate kidneys (Fig. 6*E1*). Renal tubular epithelial cells in the deep cortical layer were occasionally stained. The above data suggested that alterations in adhesive properties of tubular epithelial cells may

single normal UB, but the *Lzts2* null embryo appears a split mesenchyme (designated by *double arrows*). *D*, staining for Pax2 in wild type and *Lzts2* null embryos. The ectopic ureteric buds are marked with *arrows*.

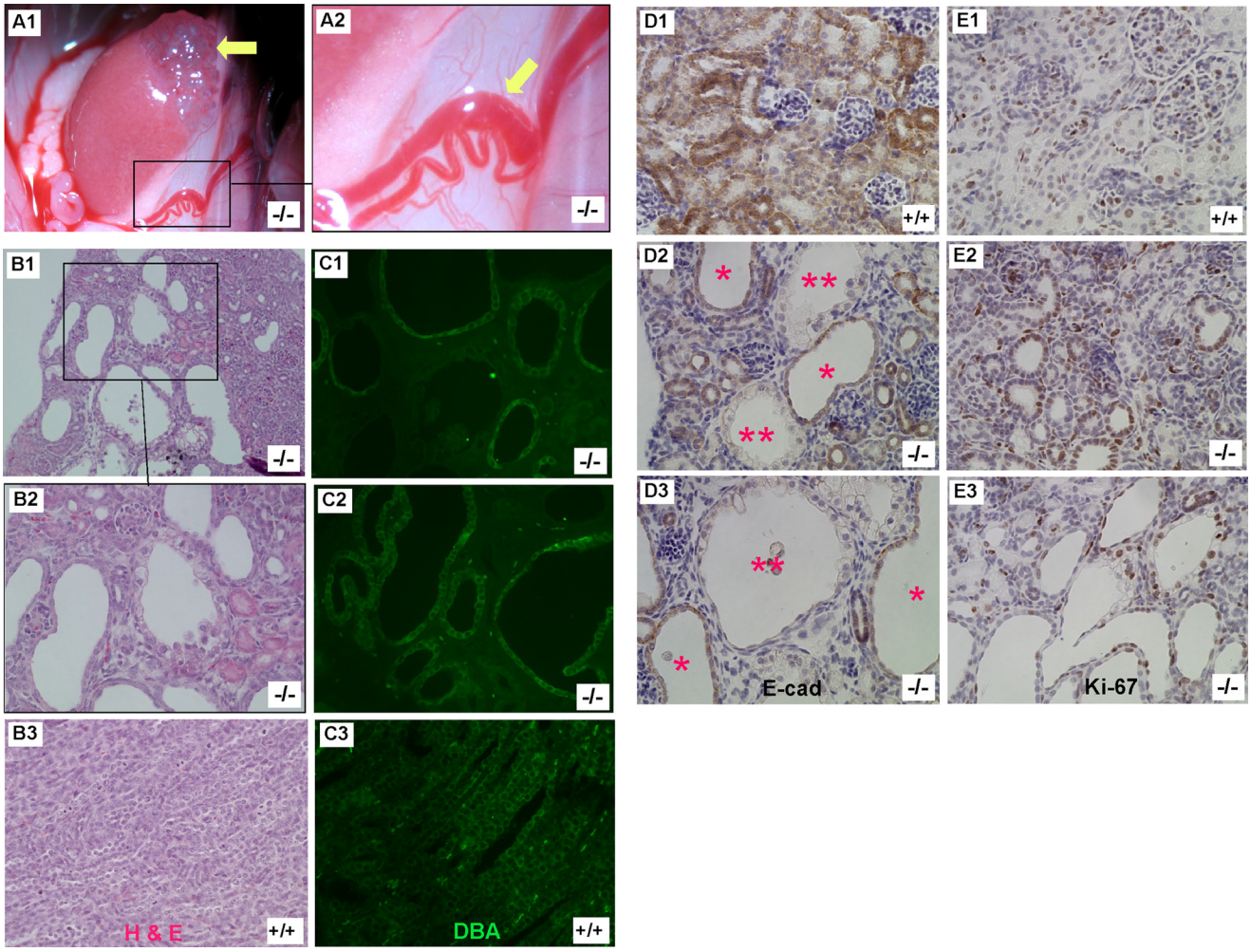

FIGURE 6. ***Lzts2* null mice displayed cystic renal dysplasia.** A representative renal cyst at lower (*A1*) and higher (*A2*) magnification in a newborn *Lzts2*$^{-/-}$ mouse showed upper pole renal polycystic changes (*yellow arrow*, *A1*) with hydroureter (*yellow arrow*, *A2*). Histological examination of the cystic kidneys was conducted, and the representative images showed multiple cyst formation in the parenchyma at low (*B1*) and high magnification (*B2*). Sex- and age-matched *Lzts2*$^{+/+}$ littermates were analyzed, and a representative image is shown (*B3*). Dolichos biflorus agglutinin (*DBA*, FITC-labeled) staining was performed and revealed that most of the epithelial cysts were mainly derived from the collecting system of the kidney in *Lzts2* null mice (*C1* and *C2*). An image from an age- and sex-matched *Lzts2*$^{+/+}$ littermate was shown (*C3*). Immunohistochemical analyses were performed with the E-cadherin antibody in the above *Lzts2*$^{+/+}$ (*D1*) and *Lzts2*$^{-/-}$ newborns (*D2* and *D3*). Whereas cysts lined by a single layer of epithelial cells (*) showed positive E-cadherin staining, cysts lined by epithelial cells with increased cytoplasm and enlarged nuclei (**) showed significantly reduced E-cadherin staining (*D2* and *D3*). The representative images of immunohistochemical staining with the Ki-67 antibody in the kidney of *Lzts2*$^{+/+}$ (*E1*) and *Lzts2*$^{-/-}$ neonate kidney tissues (*E2* and *E3*) were shown.

directly link to the pathogenesis of renal cysts in *Lzts2* null kidneys (29).

β-Catenin Subcellular Localization Was Altered in Lzts2 Null Kidneys—Wnt signaling and its key component, β-catenin, have been implicated in kidney development (11, 13, 14). Previously, we have demonstrated that LZTS2 regulates the cellular level and localization of β-catenin (5). Discovery of kidney and urinary tract anomalies in *Lzts2* null mice suggests a potential role for LZTS2 in regulating β-catenin during kidney development. Thus, we assessed whether expression of β-catenin was altered in renal tubule epithelia and collecting duct epithelia of *Lzts2* null mice. Although in wild type kidneys, β-catenin showed a defined expression on the basolateral side of the renal tubule epithelium and membrane, as well as cell-cell junctions of the collecting duct epithelium (Fig. 7, *A* and *B*), there also appeared to be increased cytoplasmic expression of β-catenin in *Lzts2* null kidneys (Fig. 7, *C* and *D*). In addition, where dysplastic renal cysts were exhibited, basolateral staining of β-catenin in lining epithelia was reduced. Furthermore, intensive nuclear staining of β-catenin was observed in mesenchyme surrounding the cysts (Fig. 7*E*). Because overexpression of a proteolysis-resistant mutant of β-catenin or conditional inactivation of APC can lead to cystic renal disease and cystic renal neoplasia in related mouse models (30, 31), the above results may suggest the role of LZTS2 in the regulation of β-catenin and its biological consequence in kidney disorders observed in *Lzts2* null mice.

To assess the effect of *Lzts2* on cellular β-catenin, we prepared mouse embryonic fibroblasts (MEFs) from the embryos at E13.5 through intercrosses between *Lzts2* heterozygous mice (*Lzts2*$^{+/-}$). Both whole cell lysates and nuclear extracts prepared from different genotypes of MEFs were analyzed for expression of Lzts2 proteins. LZTS2 was detected in whole cell lysates isolated from wild type and *Lzts2*$^{+/-}$ MEFs but not in *Lzts2* null MEFs (Fig. 7*F*). Interestingly, a notable increase of nuclear β-catenin was observed in the nuclear extract of *Lzts2*

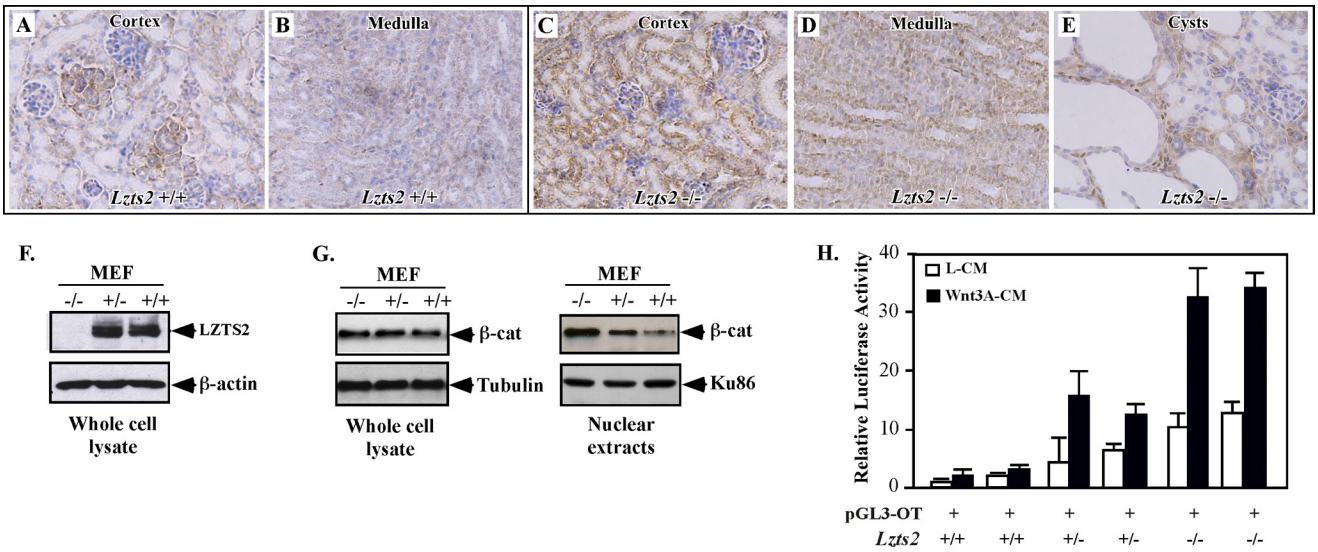

FIGURE 7. **β-Catenin subcellular localization was altered in *Lzts2* null kidneys.** *A* and *B*, staining of β-catenin in the cortex (*A*) and medulla (*B*) of wild type kidney was defined on the basolateral side of the renal tubule epithelium and membrane, as well as cell-cell junctions of the collecting duct epithelium. *C* and *D*, staining of β-catenin in the cortex and medulla of *Lzts2* null kidneys appeared more cytoplasmic than membranous. *E*, staining of β-catenin in dysplastic renal cysts of *Lzts2* null kidneys showed reduced basolateral staining but intense nuclear staining in mesenchyme surrounding the cysts. *F*, MEFs were prepared from the litter of embryos at E13.5 through intercrosses between *Lzts2* heterozygous mice ($Lzts2^{+/-}$). Whole cell lysates were prepared from different genotypes of MEFs and were analyzed to detect the expression of Lzts2 and β-catenin in Western blotting. *G*, expression of β-catenin was detected in both whole cell lysates and nuclear extracts isolated from different genotype MEFs as indicated in the figure. The specific antibody against β-catenin or Ku86, a nuclear protein marker, was used in Western bolt analyses. *H*, transient transfection experiments were carried out in different genotype MEFs. One hundred ng of Topflash (pGL3-OT) or the inactive mutant Foflash (pGL3-OF) and 25 ng of pcDNA3-β-galactosidase was transfected into each sample. The transfected cells were incubated in DMEM with 5% fetal calf serum for 24 h, then washed, and cultured with either Wnt3a-CM or L-CM for another 24 h. The cells were harvested, and the luciferase and β-galactosidase activity were measured. Luciferase activity is reported as relative light units (luciferase/β-galactosidase) and represented as the means ± S.D.

null MEFs despite levels of total β-catenin being almost similar in these cells (Fig. 7*G*). These observations were consistent with our previous results that LZTS2 promotes the nuclear export of β-catenin (5) and further elucidates that the loss of endogenous LZTS2 proteins results in accumulated nuclear β-catenin.

To examine whether LZTS2 modulates β-catenin-mediated transcription, we transfected either Topflash (OT) or Foflash (OF) reporters into the above MEFs and cultured cells in the presence of Wnt3A conditioned medium or L medium, as a control (22). As shown in Fig. 7*H*, Wnt3A-CM induced higher luciferase activity on the OT promoter in two *Lzts2* null MEF lines than in wild type and $Lzts2^{+/-}$ MEFs. There was little or no activity in the samples treated with L-CM or transfected with the OF promoter/reporter (data not shown). The above data indicate that β-catenin-mediated transcription was elevated in *Lzts2* null cells, likely through dysregulation of β-catenin cellular localization. The dysregulation of the β-catenin signaling pathway may have predisposed the kidney to subsequent malformation.

DISCUSSION

LZTS2, also named LAPSER, was originally identified as a homologue of FEZ1/LZTS1 (1). The *LZTS2* gene is located on human chromosome 10 at 10q24.3, the region that is frequently lost in human tumors (4). It has been shown that LZTS2 interacts with β-catenin and represses β-catenin-mediated T-cell factor/lymphoid-enhancing factor-mediated transcription (5). Intriguingly, a Rev-like, leucine-rich CRM1/exportin regulated nuclear exporting signal sequence was identified at the C terminus of the LZTS2. It has been demonstrated that through this nuclear export signal site, LZTS2 can regulate the cellular localization of β-catenin. To address the biological significance of LZTS2 *in vivo*, we recently generated mice with a targeted disruption of the *Lzts2* gene. Here, we report that homozygous null deletion of *Lzts2* in mice resulted in renal abnormalities resembling human CAKUT. We showed that mice homozygous for *Lzts2* knock-out allele display renal and urinary tract defects including duplication abnormalities, hydroureter, hydronephrosis, and cystic kidneys. We also demonstrated that in *Lzts2* null embryos, the UB formation was ectopic. Finally, we provided evidence to link Lzts2 to cellular localization of β-catenin in this mouse model. Our data for impaired induction of UB outgrowth at early stages during kidney development in *Lzts2* null embryos demonstrate an essential role of LZTS2 in kidney and urinary tract development.

Mouse kidney development initiates at approximately E10.5 to E11 days when the MM induces an epithelial thickening at the posterior part of the Wolffian duct known as the UB (25). As UB invades the adjacent MM, the mutual interaction between UB and MM through inductive signaling ensures the outgrowth and multiple branching of UB that eventually give rise to the renal collecting system and ureter. UB branching morphogenesis continues during the first week of postnatal development to form the definitive kidney. The initiation of appropriate outgrowth of the UB is an essential step in development of the urogenital system. Abnormal UB outgrowth leads to a variety of renal and urinary tract developmental defects including hypoplastic or dysplastic kidney, ectopic ureter, megaureter, ureteroceles, and vesicoureteral reflux (32). These phenotypes

mimic the human CAKUT that are the most common cause of renal failure in children (33, 34). In addition, we also observed renal dysplasia, cystic disease, hydronephrosis, hydroureter, and collecting system duplication in Lzts2 null embryos, neonates, and adult mice. The results suggest a critical role for LZTS2 in regulating the pathways that directly affect early renal development.

The morphogenesis of UB outgrowth is a complicated process involving both positive and negative regulatory mechanisms. Multiple lines of evidence have shown that the appropriate expression of Gdnf is a key event in UB formation (32, 35, 36). In addition to GDNF expression level, the localized or spatial expression domain of GDNF also plays an important role in kidney formation. In this study, we did not see clear abnormal Gdnf expression in *Lzts2* null mice, suggesting that the ectopic ureteric buds that form in Lzts2 mutants are the result of a misinterpretation of the GDNF/Ret signal within the Wolffian duct but are not caused by abnormal Gdnf expression. To confirm our findings, we also examined the expression of C-Ret and its downstream targets, Wnt11 and Pax2. Expression of these genes appears in the process of the ureteric budding. It will be interesting to exploit the Gdnf-independent pathways that are regulated and/or mediated through the Wnt/β-catenin pathway in early UB development.

In the current study, we characterized the *Lzts2* expression pattern during the course of kidney development in wild type and *Lzts2* null mice. We observed that *Lzts2* was expressed in the UB and developing nephron structures where β-catenin has been shown to be expressed (11). Kidney defects in *Lzts2* null mice appeared to be very similar to the abnormalities identified in β-catenin loss-of-function or gain-of-function mutations. It has been demonstrated that ablation of β-catenin in the Wolffian duct/UB epithelium cell lineage or in ureteric cell lineage resulted in a range of pathologic changes, including renal dysplasia, cystic changes, reduced ureteric bud branching, and ectopic ureters (11, 35). Although β-catenin has been shown to be essential at the onset of tubulogenesis, repression of β-catenin at a later stage is required for normal kidney development. Previous studies revealed cystic dysplasia in transgenic mice expressing an activated mutant of β-catenin (31) and in mice with conditional inactivation of *Apc* elevating cytoplasmic levels of β-catenin in renal tubular epithelium, which further results in kidney cyst formation (30). Dysregulated β-catenin cellular distribution and transcriptional activity was one underlying mechanism that explains the kidney defects in *Lzts2* null mice. We also observed expression of Lzts2 mainly in distal convoluted tubules of adult moue kidneys (supplemental Fig. S1). As noted, we did not observe gross developmental defects in other tissues of *Lzts2* null mice, including the neural tissues where *Lzts2* was highly expressed (Fig. 1). However, more subtle neural phenotypes may go undetected given the lack of specific markers in the central nervous system (37). Further analyses using tissue-specific knock-out models would be able to further define the role of Lzts2 in renal and other organogenesis.

In this study, we have searched for the potential causes of hydronephrosis and hydroureter in Lzts2 null mice. In general, hydronephrosis and hydroureter are caused by either primary congenital conditions or secondary acquired conditions. In humans and most animals, secondary acquired conditions are the most common causes, resulting usually from lower urinary tract diseases that lead to obstruction such as urolithiasis, cystitis, and urinary bladder neoplasms. In contrast, congenital hydronephrosis is a commonly observed condition in genetically unmanipulated and experimentally unmanipulated laboratory mice in general (38, 39). In most of these cases, the exact defect resulting in hydronephrosis is unknown or undetermined. In our Lzts2 null mice, we believe that the hydronephrosis and hydroureter is also congenital in origin. Occurrence of abnormal ureteral budding suggests congenital malformations of the ureter as a potential cause of hydronephrosis and hydroureter in the *Lzts2* null mice. Unfortunately, our preliminary investigations via histology failed to identify specific congenital ureteral entities that may have resulted in hydronephrosis and hydroureter, including downstream narrowing in ureter luminal diameter, or segmental/complete ureteral agenesis in *Lzts2* null mice. However, the specificity and sensitivity of detecting ureteral abnormalities in mice is low because of the size of the ureter, which makes it difficult to obtain a consistent, full-length section of the entire ureter and results in the inability to assess functional changes that could result in ureterovesical reflux. More thorough investigations are warranted to further characterize and confirm our suspicions of congenital ureteral abnormalities as a cause of hydronephrosis and hydroureter in *Lzts2* null mice.

Recently, potential roles of the LZTS protein family in cell growth and tumor formation have been suggested. *Lzts1* null mice displayed tumor phenotypes (3). However, there was no other abnormality such as renal defects in the mouse model. Although both proteins share some sequence similarity, there is no clear evidence suggesting that these proteins functionally overlap given our data showing that there is no or low expression of *Lzts1* in the early stages during kidney development. More analyses should be carried out to further define the potential role of LZTS2 as a novel regulator of the Wnt/β-catenin signaling pathway in development and tumorigenesis.

REFERENCES

1. Cabeza-Arvelaiz, Y., Thompson, T. C., Sepulveda, J. L., and Chinault, A. C. (2001) *Oncogene* **20,** 6707–6717
2. Vecchione, A., Ishii, H., Shiao, Y. H., Trapasso, F., Rugge, M., Tamburrino, J. F., Murakumo, Y., Alder, H., Croce, C. M., and Baffa, R. (2001) *Clin. Cancer Res.* **7,** 1546–1552
3. Vecchione, A., Baldassarre, G., Ishii, H., Nicoloso, M. S., Belletti, B., Petrocca, F., Zanesi, N., Fong, L. Y., Battista, S., Guarnieri, D., Baffa, R., Alder, H., Farber, J. L., Donovan, P. J., and Croce, C. M. (2007) *Cancer Cell* **11,** 275–289
4. Li, J., Yen, C., Liaw, D., Podsypanina, K., Bose, S., Wang, S. I., Puc, J., Miliaresis, C., Rodgers, L., McCombie, R., Bigner, S. H., Giovanella, B. C., Ittmann, M., Tycko, B., Hibshoosh, H., Wigler, M. H., and Parsons, R. (1997) *Science* **275,** 1943–1947
5. Thyssen, G., Li, T. H., Lehmann, L., Zhuo, M., Sharma, M., and Sun, Z. (2006) *Mol. Cell. Biol.* **26,** 8857–8867
6. Teufel, A., Weinmann, A., Galle, P. R., and Lohse, A. W. (2005) *Oncol. Rep.* **14,** 547–551
7. Hyun Hwa, C., Hye Joon, J., Ji Sun, S., Yong Chan, B., and Jin Sup, J. (2008) *Biochim. Biophys. Acta* **1783,** 419–428
8. Schmeisser, M. J., Grabrucker, A. M., Bockmann, J., and Boeckers, T. M. (2009) *J. Biol. Chem.* **284,** 29146–29157

9. Sudo, H., and Maru, Y. (2007) *FASEB J.* **21,** 2086–2100
10. Sudo, H., and Maru, Y. (2008) *Hum. Mol. Genet.* **17,** 2524–2540
11. Bridgewater, D., Cox, B., Cain, J., Lau, A., Athaide, V., Gill, P. S., Kuure, S., Sainio, K., and Rosenblum, N. D. (2008) *Dev. Biol.* **317,** 83–94
12. Iglesias, D. M., Hueber, P. A., Chu, L., Campbell, R., Patenaude, A. M., Dziarmaga, A. J., Quinlan, J., Mohamed, O., Dufort, D., and Goodyer, P. R. (2007) *Am. J. Physiol. Renal Physiol.* **293,** F494–F500
13. Marose, T. D., Merkel, C. E., McMahon, A. P., and Carroll, T. J. (2008) *Dev. Biol.* **314,** 112–126
14. Park, J. S., Valerius, M. T., and McMahon, A. P. (2007) *Development* **134,** 2533–2539
15. Rodríguez, C. I., Buchholz, F., Galloway, J., Sequerra, R., Kasper, J., Ayala, R., Stewart, A. F., and Dymecki, S. M. (2000) *Nat. Genet.* **25,** 139–140
16. Lakso, M., Sauer, B., Mosinger, B., Jr., Lee, E. J., Manning, R. W., Yu, S. H., Mulder, K. L., and Westphal, H. (1992) *Proc. Natl. Acad. Sci. U.S.A.* **89,** 6232–6236
17. Sharma, M., Li, X., Wang, Y., Zarnegar, M., Huang, C. Y., Palvimo, J. J., Lim, B., and Sun, Z. (2003) *EMBO J.* **22,** 6101–6114
18. Beliakoff, J., Lee, J., Ueno, H., Aiyer, A., Weissman, I. L., Barsh, G. S., Cardiff, R. D., and Sun, Z. (2008) *Mol. Cell. Biol.* **28,** 282–292
19. Mahoney, Z. X., Sammut, B., Xavier, R. J., Cunningham, J., Go, G., Brim, K. L., Stappenbeck, T. S., Miner, J. H., and Swat, W. (2006) *Proc. Natl. Acad. Sci. U.S.A.* **103,** 19872–19877
20. Gray, P. A., Fu, H., Luo, P., Zhao, Q., Yu, J., Ferrari, A., Tenzen, T., Yuk, D. I., Tsung, E. F., Cai, Z., Alberta, J. A., Cheng, L. P., Liu, Y., Stenman, J. M., Valerius, M. T., Billings, N., Kim, H. A., Greenberg, M. E., McMahon, A. P., Rowitch, D. H., Stiles, C. D., and Ma, Q. (2004) *Science* **306,** 2255–2257
21. Peng, Y., Lee, J., Zhu, C., and Sun, Z. (2010) *J. Biol. Chem.* **285,** 11465–11475
22. Verras, M., Brown, J., Li, X., Nusse, R., and Sun, Z. (2004) *Cancer Res.* **64,** 8860–8866
23. Kobayashi, A., Kwan, K. M., Carroll, T. J., McMahon, A. P., Mendelsohn, C. L., and Behringer, R. R. (2005) *Development* **132,** 2809–2823
24. Ichikawa, I., Kuwayama, F., Pope, J. C., 4th, Stephens, F. D., and Miyazaki, Y. (2002) *Kidney Int.* **61,** 889–898
25. Saxén, L., and Sariola, H. (1987) *Pediatr. Nephrol.* **1,** 385–392
26. Pachnis, V., Mankoo, B., and Costantini, F. (1993) *Development* **119,** 1005–1017
27. Rosenthal, A. (1999) *Neuron* **22,** 201–203
28. Sainio, K., Suvanto, P., Davies, J., Wartiovaara, J., Wartiovaara, K., Saarma, M., Arumäe, U., Meng, X., Lindahl, M., Pachnis, V., and Sariola, H. (1997) *Development* **124,** 4077–4087
29. Basson, M. A., Watson-Johnson, J., Shakya, R., Akbulut, S., Hyink, D., Costantini, F. D., Wilson, P. D., Mason, I. J., and Licht, J. D. (2006) *Dev. Biol.* **299,** 466–477
30. Qian, C. N., Knol, J., Igarashi, P., Lin, F., Zylstra, U., Teh, B. T., and Williams, B. O. (2005) *J. Biol. Chem.* **280,** 3938–3945
31. Saadi-Kheddouci, S., Berrebi, D., Romagnolo, B., Cluzeaud, F., Peuchmaur, M., Kahn, A., Vandewalle, A., and Perret, C. (2001) *Oncogene* **20,** 5972–5981
32. Costantini, F., and Shakya, R. (2006) *Bioessays* **28,** 117–127
33. Chen, F. (2009) *Pediatr. Nephrol.* **24,** 1621–1632
34. Kerecuk, L., Schreuder, M. F., and Woolf, A. S. (2008) *Nat. Clin. Pract. Nephrol.* **4,** 312–325
35. Moore, M. W., Klein, R. D., Fariñas, I., Sauer, H., Armanini, M., Phillips, H., Reichardt, L. F., Ryan, A. M., Carver-Moore, K., and Rosenthal, A. (1996) *Nature* **382,** 76–79
36. Pichel, J. G., Shen, L., Sheng, H. Z., Granholm, A. C., Drago, J., Grinberg, A., Lee, E. J., Huang, S. P., Saarma, M., Hoffer, B. J., Sariola, H., and Westphal, H. (1996) *Nature* **382,** 73–76
37. Dressler, G. R., Wilkinson, J. E., Rothenpieler, U. W., Patterson, L. T., Williams-Simons, L., and Westphal, H. (1993) *Nature* **362,** 65–67
38. Percy, B. S. (2007) in *Mouse*, 3rd Ed., Blackwell Publishing, Ames, IA
39. Peters, C. A. (2001) *Prenat. Diagn.* **21,** 917–923